Lifetimes of $4p^5 4d$ levels in highly ionized atoms

Gediminas Gaigalas and Pavel Rynkun*
Vilnius University, Institute of Theoretical Physics and Astronomy, A. Goštauto 12, LT-01108, Vilnius, Lithuania

Charlotte Froese Fischer
National Institute of Standards and Technology, Gaithersburg, Maryland 20899, USA
(Received 18 November 2014; published 17 February 2015)

Energy levels, lifetimes, and wave function compositions have been computed for all atomic states of the $4p^6$ and $4p^5 4d$ configurations using the multiconfiguration Dirac-Hartree-Fock method. Calculations were done by parity and the configuration state function expansions were obtained by allowing single and double substitutions from the the $4p^6$ and $4p^5 4d$ single references with orbitals in an orbital set that was extended to $n = 7$ and all possible angular symmetries. Lifetimes are computed from $E1$, $E2$, and $M1$ transitions between these levels. Energy levels and transition energies (or wavelengths) are compared with other theory and experiment, when available. Transition data for the $4p^6\ ^1S_0 - 4p^5\,4d\ J = 1$ transitions are investigated in detail with respect to convergence of transition energies and the length and velocity forms of the line strengths. By classifying the upper states by J, parity (π), and position, the compositions of the states with the same three quantum number change smoothly as a function of the nuclear charge Z and transition energies and transition matrix elements can be approximated by polynomial expressions in Z. A zero in the transition matrix element for the $^1S_0$ - $^3P_1^o$ transition leads to a long lifetime at $Z \approx 58$.

DOI: 10.1103/PhysRevA.91.022509 PACS number(s): 31.15.ag, 31.15.aj, 31.15.am

I. INTRODUCTION

Currently tungsten (W) is an element of great interest as a plasma wall material for future tokamaks and more spectroscopic data are available for its ions than any other element in a similar region of the periodic table. Wavelengths and intensities of prominent lines in electron-beam ion-trap (EBIT) spectra of Rb-like W^{37+} to Cu-like W^{45+} ions were measured by Utter *et al.* [1]. More recently the range has been extended by Ralchenko *et al.* [2] from In-like W^{25+} to Co-like W^{47+} and from I-like W^{21+} to V-like W^{51+} by Radtke *et al.* [3].

From a theoretical perspective, much can be learned about atomic structure from a study of isoelectronic sequences where only the atomic number Z varies and trends are continuous functions of Z. The calibration of accuracy of computed energy levels can be based on a few experimental values and applied to a computational study of nearby elements in the sequence. In this paper, these ideas are applied to lifetimes of the $4s^2\,4p^5\,4d$ levels of the Kr-like sequence from Xe^{18+} ($Z = 54$) to Au^{43+} ($Z = 79$). Experimental data are available for several of these spectra.

Breton *et al.* [4] reported spectra of xenon (Xe) ions obtained from ohmically heated TFR tokamak plasmas and performed *ab initio* calculations. Biedermann *et al.* [5] observed lines in EBIT spectra for Rb-like Xe^{17+} to Cu-like Xe^{25+}. Kato *et al.* [6] measured EUV spectra of xenon ions from the large helical device (LHD). Crespo *et al.* [7] measured transitions in highly charged ions of Kr, Xe, and Ba at the Lawrence Livermore National Laboratory EBIT. Sugar *et al.* [8] observed lines of the $4s^2\,4p^6\ ^1S_0 - 4s^2\,4p^5\,4d\ ^1P_1^o$ and $^3D_1^o$ transitions in Kr-like ions using radiation from the TEXT tokamak.

Draganić *et al.* [9] observed EUV lines of highly charged Hf, Ta, and Au ions in EBIT spectra. They used collisional-radiative (CR) modeling of the EBIT plasma to identify observed lines. Träbert *et al.* [10] studied spectra of highly charged Au ions in an EBIT and performed calculations using the relativistic HULLAC package.

In this work calculations were performed for the even parity $4s^2 4p^6$ ground state and the odd parity $4s^2\,4p^5\,4d$ excited states in Xe^{18+}, Cs^{19+}, Ba^{20+}, Ce^{22+}, Gd^{28+}, Hf^{36+}, W^{38+}, and Au^{43+}. Lifetimes and transition probabilities for $E1$, $E2$, $M1$ transitions between these levels are reported ($E2$ and $M1$ data are available as Supplemental Material [11]). Accuracy is estimated by comparing the computed wavelengths with those derived from observation and the agreement of length and velocity transition rates for $E1$ and $E2$ transitions. For the $4p^6\ ^1S_0 - 4p^5\,4d\ J = 1$ transitions, transition energies and transition matrix elements are investigated and plotted as functions of Z. From the quantities above the lifetime trends of the $4p^5\,4d\ J = 1$ states were obtained as functions of $1/(Z - 35)$.

All calculations were performed using the general relativistic atomic structure package GRASP2K [12].

II. METHOD OF CALCULATION AND RESULTS

The GRASP2K package [12] is based on the multiconfiguration Dirac-Hartree-Fock (MCDHF) method taking into account Breit and quantum electrodynamic (QED) corrections [13,14].

In this approach, an atomic state function (ASF) Ψ of parity π and total angular momentum J, is given by a linear combination of configuration state functions (CSFs) with the same parity, $\Phi(\gamma_i \pi J)$ as

$$\Psi(\gamma \pi J) = \sum_i c_i \Phi(\gamma_i \pi J). \quad (1)$$

*pavel.rynkun@tfai.vu.lt

The multiconfiguration energy functional for this approximation is based on the Dirac-Coulomb Hamiltonian, namely (in a.u.)

$$H_{\rm DC} = \sum_{j=1}^{N}[c\boldsymbol{\alpha}_j \boldsymbol{p}_j + (\beta_j - 1)c^2 + V(r_j)] + \sum_{j<k}\frac{1}{r_{jk}}, \quad (2)$$

where $\boldsymbol{\alpha}$ and β are 4×4 Dirac matrices, $\boldsymbol{p}$ is the momentum operator, and $V(r_j)$ and $1/r_{jk}$ are the electrostatic electron-nucleus and electron-electron interactions, respectively. In all the calculations reported here, the nuclear charge distribution was modeled by the two-component Fermi function [15]. The mass numbers, that determine the nuclear parameters, used in the calculations are as follows: 131 (Xe), 133 (Cs), 137 (Ba), 140 (Ce), 157 (Gd), 179 (Hf), 184 (W), 197 (Au). A variational method [14,16] was used to optimize both the large and small components of the radial functions that define the CSFs and the expansion coefficients over the CSF basis.

As a final step, a relativistic configuration interaction (RCI) calculation was performed to include the transverse-photon (Breit) interaction describing the transversely polarized photon contribution to the electron-electron interactions in the Coulomb gauge, the vacuum polarization (VP), and the self-energy (SE) corrections to the interaction matrix. Thus the corrections affect the wave function.

Once reliable ASFs have been obtained, radiative transition probabilities, oscillator strengths, and line strengths can be determined. The transition rate (A) between two states $\gamma'\pi' J'$ (final) and $\gamma\pi J$ can be expressed in terms of the transition matrix element (ME)

$$\langle\Psi(\gamma\pi J)\|\mathbf{T}\|\Psi(\gamma'\pi' J')\rangle = \sum_{j,k} c_j c'_k \,\langle\Phi(\gamma_j\pi J)\|\mathbf{T}\|\Phi(\gamma'_k\pi' J')\rangle, \quad (3)$$

where $\mathbf{T}$ is a transition operator that depends on the type of the transition. Then

$$A = \frac{2\,(2J+1)\,\Delta E}{c\,(2k+1)\,(2J'+1)}|\langle\Psi(\gamma\pi J)\|\mathbf{T}\|\Psi(\gamma'\pi' J')\rangle|^2. \quad (4)$$

For electric multipole transitions there are two commonly used forms of the transition operator, namely, the length (Babushkin) and velocity (Coulomb) forms [17].

For transition probability calculations the important accuracy indicators [18,19] are the accuracy of the transition energies, obtained by comparison with observed data, and the agreement in the length and velocity forms of the line strength [20] for electric multipole transitions. In the present work, we report a closely related factor, namely $\delta T = |A_l - A_v|/\max(A_l, A_v)$, where A_l is the transition rate in the Babushkin (length) gauge and A_v in the Coulomb (velocity) gauge.

For the construction of the ASFs the SR-SD method was used. In this approach the CSFs that form the basis for the the multiconfiguration expansion of Eq. (1) included all single and double (SD) substitutions from the valence shells outside the inactive core of the single configuration in the reference set. Unless stated otherwise, in the present calculations the inactive core was $1s^2\,2s^2\,2p^6\,3s^2\,3p^6\,3d^{10}$. SD substitutions were performed from the even $4s^2\,4p^6$ configuration with $J = 0$, and from the $4s^2\,4p^5\,4d$ odd configuration with CSFs for $J = 0,1,2,3,4$ to orbital sets with principal quantum numbers $n = 4,\ldots,7$, respectively, and all possible angular symmetries. Table I summarizes the calculations performed for each group of levels by showing their J and π values, the ASFs that were included in the optimization process, and the size of the wave-function expansion for the $n = 7$ results.

TABLE I. Summary of the extended optimal level MCDHF calculations performed indicating the range of eigenvalues and the size of the final interaction matrix for each J of the group for the $n = 7$ orbital set.

J	Parity	Eigenvalues	Size
0	+	1	1 502
0	−	1	22 334
1	−	1–3	63 516
2	−	1–4	95 051
3	−	1–3	113 150
4	−	1	116 953

Table II shows the convergence of transition data for Xe^{18+} ($Z = 54$) and W^{38+} ($Z = 74$) as the size of the orbital set increases. As a check on the validity of the assumption that $3d^{10}$ can be part of an inactive core, calculations were performed for Xe^{18+} allowing double substitutions from $3d^{10}$ to represent core correlation (CC) and single or double substitutions with only one substitution from $3d^{10}$ and one from the valence subshells, referred to as core-valence (CV) correlation. Inclusion of these substitutions up to $n = 6$ and then again closing the $3d^{10}$ subshell for $n = 7$ contributions, increased the size of the expansion for the $J = 1$ state from 63 516 to 266 215, a significant increase. Results accounting for CC + CV correlation are included in Table II. By comparing the wavelength from both calculations with the same n, it is clear the changes for opening the $3d$ shell are generally less than 0.5% in the wavelength but CC + CV affects the line strength up to 7%, depending on the transition. Except for the transition to $^3P_1^o$, where the calculation of the transition matrix element is accompanied by a significant cancellation, there is a decrease in δT with an increase in n, particularly for the CC + CV calculation indicating an improvement in accuracy. At the same time, the values for δT are somewhat larger, especially in the presence of cancellation. The importance of the CC + CV corrections decreases with the degree of ionization.

In the MCDHF formalism, the CSFs are constructed from nl_- and nl_+ orbitals that are coupled in jj coupling to a final J quantum number. By assuming the radial functions are the same nl orbitals, an expansion in a jj-coupled basis of CSFs can be transformed to the more common LSJ basis using the newly developed JJ2LSJ program, part of the latest version (v3) of the GRASP2K code [12].

Table III reports computed $4p^5 4d$ energy levels relative to the $4p^6$ ground state, lifetimes, and wave-function compositions of ASFs in LSJ coupling. Labels for ASFs usually are assigned as the label of the CSF making the largest contribution to the composition. However, such labels may not be unique. An algorithm that has been proposed for assigning unique labels [21] starts with a set of, say m ASFs of the same πJ and the m CSFs with large expansion coefficients. Of the set

TABLE II. Convergence of transition data in Xe^{18+} and W^{38+} for $E1$ transitions: wavelength λ (in Å), line strength S (length form), weighted oscillator strength gf (length form), transition rate A_{ki} (length form) in s^{-1}, δT accuracy indicator. $n = 5$ corresponds to calculations allowing SD substitutions from valence shells. $n = 5$ CC + CV corresponds to calculations allowing D substitutions from $3d^{10}$ to represent core correlation (CC) and SD substitutions with only one substitution from $3d^{10}$ and one from the valence subshells, referred to as core-valence (CV) correlation.

n	λ (Å)	S	gf	A_{ki} (s^{-1})	δT
Xe^{18+} ($Z = 54$)					
	$4p^6\ {}^1S_0 - 4p^5 4d\ {}^3P_1^o$				
4	151.83	1.915×10^{-4}	3.831×10^{-4}	3.695×10^{7}	0.159
5	152.08	1.730×10^{-4}	3.456×10^{-4}	3.322×10^{7}	0.001
6	152.30	1.763×10^{-4}	3.516×10^{-4}	3.370×10^{7}	0.095
7	152.32	1.787×10^{-4}	3.564×10^{-4}	3.415×10^{7}	0.072
5 CC + CV	151.59	1.776×10^{-4}	3.559×10^{-4}	3.444×10^{7}	0.276
6 CC + CV	152.00	1.899×10^{-4}	3.796×10^{-4}	3.653×10^{7}	0.237
7 CC + CV	152.09	1.895×10^{-4}	3.785×10^{-4}	3.638×10^{7}	0.229
	$4p^6\ {}^1S_0 - 4p^5 4d\ {}^3D_1^o$				
4	130.84	1.390×10^{-1}	3.228×10^{-1}	4.192×10^{10}	0.024
5	131.12	1.449×10^{-1}	3.358×10^{-1}	4.342×10^{10}	0.006
6	131.38	1.473×10^{-1}	3.406×10^{-1}	4.387×10^{10}	0.016
7	131.43	1.483×10^{-1}	3.427×10^{-1}	4.411×10^{10}	0.008
5 CC + CV	130.77	1.493×10^{-1}	3.468×10^{-1}	4.509×10^{10}	0.076
6 CC + CV	131.14	1.527×10^{-1}	3.538×10^{-1}	4.574×10^{10}	0.067
7 CC + CV	131.33	1.565×10^{-1}	3.620×10^{-1}	4.667×10^{10}	0.042
	$4p^6\ {}^1S_0 - 4p^5 4d\ {}^1P_1^o$				
4	106.30	1.444	4.127	8.122×10^{11}	0.026
5	106.73	1.469	4.180	8.160×10^{11}	0.012
6	107.00	1.470	4.172	8.103×10^{11}	0.020
7	107.06	1.472	4.178	8.105×10^{11}	0.013
5 CC + CV	107.07	1.392	3.948	7.657×10^{11}	0.057
6 CC + CV	107.44	1.395	3.945	7.599×10^{11}	0.053
7 CC + CV	107.73	1.402	3.952	7.572×10^{11}	0.035
W^{38+} ($Z = 74$)					
	$4p^6\ {}^1S_0 - 4p^5 4d\ {}^3P_1^o$				
4	80.56	1.950×10^{-3}	7.351×10^{-3}	2.518×10^{9}	0.033
5	80.59	2.042×10^{-3}	7.698×10^{-3}	2.636×10^{9}	0.056
6	80.67	2.027×10^{-3}	7.631×10^{-3}	2.607×10^{9}	0.049
7	80.68	2.036×10^{-3}	7.666×10^{-3}	2.619×10^{9}	0.055
	$4p^6\ {}^1S_0 - 4p^5 4d\ {}^3D_1^o$				
4	63.49	2.362×10^{-1}	1.130	6.233×10^{11}	0.020
5	63.51	2.381×10^{-1}	1.139	6.277×10^{11}	0.010
6	63.62	2.392×10^{-1}	1.142	6.274×10^{11}	0.004
7	63.64	2.397×10^{-1}	1.144	6.281×10^{11}	0.007
	$4p^6\ {}^1S_0 - 4p^5 4d\ {}^1P_1^o$				
4	46.36	3.318×10^{-1}	2.174	2.249×10^{12}	0.008
5	46.39	3.340×10^{-1}	2.187	2.259×10^{12}	0.003
6	46.44	3.335×10^{-1}	2.181	2.248×10^{12}	0.002
7	46.45	3.337×10^{-1}	2.182	2.248×10^{12}	0.0004

of CSFs, the one with the largest expansion coefficient of all m ASFs defines the label of the ASF in which it occurs. The labeled ASF and the associated CSF are eliminated from further consideration. Each assignment gives the CSFs with the largest expansion coefficient to an ASF as the label. In this scheme, the last remaining label may be based on a contribution that is not the largest, as seen, for example, for the level at 709 633 cm^{-1} labeled $4p^5 4d\ {}^3P_2^o$ for Cs^{19+} in Table III. It may also happen that two compositions are very nearly equal making the order sensitive to the calculations. In Table III the $^3D_2^o$ composition in Ba^{20+} for the level at 739 587 cm^{-1} is only marginally larger than for the level at 915 437 cm^{-1}, namely 45.67% vs 45.61%. With such a definition, atomic properties for an isoelectronic sequence with a specific label may not be continuous or smooth.

Table IV reports the $n = 7$ results for $E1$ transitions from the $4p^6\ {}^1S_0$ ground state to the odd $4p^5 4d$ excited levels with $J = 1$ for the ions Xe^{18+}, Cs^{19+}, Ba^{20+}, Ce^{22+}, Gd^{28+}, Hf^{36+}, W^{38+}, and Au^{43+}. Similar tables for all electric quadrupole ($E2$) and magnetic dipole ($M1$) transitions

TABLE III. Energy levels (in cm^{-1}), lifetimes (in s), and wave function composition of the $4s^2\,4p^5\,4d$ levels in LSJ coupling for Xe^{18+}, Cs^{19+}, Ba^{20+}, Ce^{22+}, Gd^{28+}, Hf^{36+}, W^{38+}, and Au^{43+} with unique labels. Included as part of the label is the position of the level in the $(\pi\ J)$ group of states.

Label	POS	Level (cm^{-1})	Lifetimes (s)	Composition (%) LSJ coupling
		Xe^{18+}		
$4p^5 4d\ ^3P_0^o$	1	643 677		**97**
$^3P_1^o$	1	656 503	2.93×10^{-8}	**86** + **12** ^3D
$^3F_3^o$	1	678 448	2.57×10^{3}	**65** + **23** ^1F + **9** ^3D
$^3P_2^o$	1	679 577	6.75×10^{-3}	**46** + **41** ^3D + **10** ^3F
$^3F_4^o$	1	687 058	1.16×10^{-1}	**97**
$^1D_2^o$	2	696 303	5.57×10^{-3}	**49** + **23** ^3F + **22** ^3P + **3** ^3D
$^3D_3^o$	2	722 558	1.56×10^{-3}	**63** + **34** ^1F
$^3D_1^o$	2	760 862	2.27×10^{-11}	**78** + **11** ^3P + **8** ^1P
$^3F_2^o$	3	794 906	3.49×10^{-5}	**62** + **29** ^1D + **5** ^3D
$^3D_2^o$	4	821 680	3.68×10^{-5}	**47** + **29** ^3P + **19** ^1D + **2** ^3F
$^1F_3^o$	3	832 615	2.62×10^{-5}	**40** + **32** ^3F + **25** ^3D
$^1P_1^o$	3	934 077	1.23×10^{-12}	**88** + **7** ^3D + **1** ^3P
		Cs^{19+}		
$4p^5 4d\ ^3P_0^o$	1	671 584		**98**
$^3P_1^o$	1	685 392	4.49×10^{-8}	**85** + **13** ^3D
$^3F_3^o$	1	707 787	2.91×10^{3}	**64** + **24** ^1F + **9** ^3D
$^3P_2^o$	1	709 633	6.04×10^{-3}	**41** + **44** ^3D + **12** ^3F + **1** ^1D
$^3F_4^o$	1	718 752	5.68×10^{-2}	**98**
$^1D_2^o$	2	728 027	3.76×10^{-3}	**49** + **26** ^3P + **21** ^3F + **2** ^3D
$^3D_3^o$	2	755 502	1.21×10^{-3}	**63** + **34** ^1F
$^3D_1^o$	2	797 487	1.85×10^{-11}	**76** + **11** ^3P + **10** ^1P
$^3F_2^o$	3	838 052	2.48×10^{-5}	**63** + **29** ^1D + **5** ^3D
$^3D_2^o$	4	867 832	2.61×10^{-5}	**46** + **30** ^3P + **18** ^1D + **3** ^3F
$^1F_3^o$	3	879 358	5.90×10^{-5}	**40** + **33** ^3F + **25** ^3D
$^1P_1^o$	3	979 429	1.16×10^{-12}	**87** + **8** ^3D + **1** ^3P
		Ba^{20+}		
$4p^5 4d\ ^3P_0^o$	1	699 462		**98**
$^3P_1^o$	1	714 277	8.63×10^{-8}	**84** + **13** ^3D
$^3F_3^o$	1	737 086	3.31×10^{3}	**64** + **25** ^1F + **9** ^3D
$^3D_2^o$	1	739 587	5.51×10^{-3}	**45.67** + **37** ^3P + **13** ^3F + **2** ^1D
$^3F_4^o$	1	750 685	3.01×10^{-2}	**98**
$^1D_2^o$	2	760 047	2.59×10^{-3}	**49** + **29** ^3P + **18** ^3F + **1** ^3D
$^3D_3^o$	2	788 678	9.46×10^{-4}	**64** + **33** ^1F
$^3D_1^o$	2	834 472	1.52×10^{-11}	**74** + **12** ^3P + **11** ^1P
$^3F_2^o$	3	882 378	1.78×10^{-5}	**63** + **28** ^1D + **5** ^3D
$^3P_2^o$	4	915 437	1.87×10^{-5}	**31** + **45.61** ^3D + **18** ^1D + **3** ^3F
$^1F_3^o$	3	927 547	1.38×10^{-5}	**39** + **33** ^3F + **25** ^3D
$^1P_1^o$	3	1 025 736	1.10×10^{-12}	**86** + **9** ^3D + **2** ^3P
		Ce^{22+}		
$4p^5 4d\ ^3P_0^o$	1	755 178		**98**
$^3P_1^o$	1	772 074	2.92×10^{-5}	**83** + **15** ^3D
$^3F_3^o$	1	795 603	4.35×10^{3}	**62** + **26** ^1F + **9** ^3D
$^3D_2^o$	1	799 241	4.78×10^{-3}	**48** + **30** ^3P + **15** ^3F + **4** ^1D
$^3F_4^o$	1	815 371	1.00×10^{-2}	**98**
$^1D_2^o$	2	825 065	1.31×10^{-3}	**49** + **34** ^3P + **15** ^3F
$^3D_3^o$	2	855 829	5.79×10^{-4}	**64** + **33** ^1F
$^3D_1^o$	2	909 560	1.05×10^{-11}	**70** + **14** ^1P + **13** ^3P
$^3F_2^o$	3	974 888	9.41×10^{-6}	**65** + **27** ^1D + **5** ^3D + **1** ^3P
$^3P_2^o$	4	1 015 396	9.89×10^{-6}	**33** + **44** ^3D + **17** ^1D + **3** ^3F
$^1F_3^o$	3	1 028 657	7.54×10^{-6}	**38** + **35** ^3F + **24** ^3D
$^1P_1^o$	3	1 121 660	9.84×10^{-13}	**83** + **12** ^3D + **2** ^3P

TABLE III. (*Continued*.)

Label	POS	Level (cm^{-1})	Lifetimes (s)	Composition (%) LSJ coupling
		Gd^{28+}		
$4p^5 4d\ ^3P_0^o$	1	922 496		**98**
$^3P_1^o$	1	946 151	5.03×10^{-9}	**79** + **19** ^3D
$^3F_3^o$	1	972 767	7.55×10^{3}	**60** + **30** ^1F + **8** ^3D
$^3D_2^o$	1	977 232	3.65×10^{-3}	**51** + **19** ^3P + **18** ^3F + **10** ^1D
$^3F_4^o$	1	1 017 733	8.98×10^{-4}	**98**
$^1D_2^o$	2	1 029 254	2.34×10^{-4}	**47** + **41** ^3P + **9** ^3F + **1** ^3D
$^3D_3^o$	2	1 067 195	1.35×10^{-4}	**66** + **31** ^1F + **1** ^3F
$^3D_1^o$	2	1 144 260	4.30×10^{-12}	**58** + **24** ^1P + **15** ^3P
$^3F_2^o$	3	1 289 582	1.68×10^{-6}	**68** + **25** ^1D + **4** ^3D + **1** ^3P
$^3P_2^o$	4	1 360 749	1.73×10^{-6}	**37** + **42** ^3D + **16** ^1D + **3** ^3F
$^1F_3^o$	3	1 378 985	1.41×10^{-6}	**37** + **38** ^3F + **24** ^3D
$^1P_1^o$	3	1 444 000	7.34×10^{-13}	**73** + **20** ^3D + **4** ^3P
		Hf^{36+}		
$4p^5 4d\ ^3P_0^o$	1	1 147 707		**98**
$^3P_1^o$	1	1 181 345	5.48×10^{-10}	**74** + **24** ^3D
$^3F_3^o$	1	1 206 705	3.51×10^{4}	**57** + **33** ^1F + **8** ^3D
$^3D_2^o$	1	1 215 365	2.88×10^{-3}	**52** + **19** ^3F + **14** ^1D + **13** ^3P
$^3F_4^o$	1	1 315 816	6.58×10^{-5}	**98**
$^1D_2^o$	2	1 328 932	3.40×10^{-5}	**46** + **43** ^3P + **6** ^3F + **3** ^3D
$^3D_3^o$	2	1 371 619	2.47×10^{-5}	**67** + **30** ^1F + **1** ^3F
$^3D_1^o$	2	1 482 658	1.87×10^{-12}	**43** + **37** ^1P + **17** ^3P
$^3F_2^o$	3	1 825 946	2.26×10^{-7}	**70** + **23** ^1D + **4** ^3D + **2** ^3P
$^3P_2^o$	4	1 962 987	2.29×10^{-7}	**41** + **39** ^3D + **15** ^1D + **3** ^3F
$^1F_3^o$	3	1 983 759	5.61×10^{-7}	**35** + **40** ^3F + **23** ^3D
$^1P_1^o$	3	1 990 060	4.95×10^{-13}	**60** + **30** ^3D + **7** ^3P
		W^{38+}		
$4p^5 4d\ ^3P_0^o$	1	1 203 118		**98**
$^3P_1^o$	1	1 239 448	3.82×10^{-10}	**73** + **25** ^3D
$^3F_3^o$	1	1 264 594	4.82×10^{4}	**57** + **34** ^1F + **8** ^3D
$^3D_2^o$	1	1 273 846	2.78×10^{-3}	**52** + **19** ^3F + **15** ^1D + **12** ^3P
$^3F_4^o$	1	1 392 887	4.08×10^{-5}	**99**
$^1D_2^o$	2	1 408 445	2.20×10^{-5}	**46** + **43** ^3P + **6** ^3F + **4** ^3D
$^3D_3^o$	2	1 452 685	1.64×10^{-5}	**68** + **29** ^1F + **1** ^3F
$^3D_1^o$	2	1 571 375	1.59×10^{-12}	**40.43** + **39.98** ^1P + **18** ^3P
$^3F_2^o$	3	1 985 683	1.43×10^{-7}	**70** + **22** ^1D + **4** ^3D + **2** ^3P
$^3P_2^o$	4	2 144 754	1.44×10^{-7}	**42** + **39** ^3D + **15** ^1D + **3** ^3F
$^1P_1^o$	3	2 152 772	4.45×10^{-13}	**57** + **32** ^3D + **8** ^3P
$^1F_3^o$	3	2 166 530	1.31×10^{-7}	**35** + **40** ^3F + **23** ^3D
		Au^{43+}		
$4p^5 4d\ ^3P_0^o$	1	1 348 036		**99**
$^3P_1^o$	1	1 391 178	1.81×10^{-10}	**70** + **28** ^3D
$^3F_3^o$	1	1 415 947	9.54×10^{4}	**56** + **35** ^1F + **8** ^3D
$^3D_2^o$	1	1 426 637	2.51×10^{-3}	**53** + **19** ^3F + **16** ^1D + **11** ^3P
$^3F_4^o$	1	1 607 810	1.24×10^{-5}	**99**
$^1D_2^o$	2	1 625 626	7.82×10^{-6}	**46** + **43** ^3P + **5** ^3F + **4** ^3D
$^3D_3^o$	2	1 673 752	6.20×10^{-6}	**68** + **29** ^1F + **1** ^3F
$^3D_1^o$	2	1 810 172	1.11×10^{-12}	**34** + **46** ^1P + **19** ^3P
$^3F_2^o$	3	2 450 705	4.80×10^{-8}	**71** + **22** ^1D + **4** ^3D + **2** ^3P
$^1P_1^o$	3	2 625 890	3.30×10^{-13}	**52** + **37** ^3D + **10** ^3P
$^3P_2^o$	4	2 676 660	4.81×10^{-8}	**43** + **38** ^3D + **14** ^1D + **3** ^3F
$^1F_3^o$	3	2 700 923	1.17×10^{-7}	**34** + **41** ^3F + **23** ^3D

between the odd levels are available as supplemental data. In all cases, the accuracy indicator δT is largest for transitions to $^3P_1^o$ where the transition rate is smaller by 2–4 orders of magnitude compared with the transitions to $^1P_1^o$. The uncertainty in δT changed from 0.01345 to 0.01344 when a point nucleus was used showing that the transition probability results are not sensitive to the nuclear model.

TABLE IV. Transition data for $E1$ transitions from the ground state to $J = 1$ levels from $n = 7$ calculations: wavelength λ (in Å), line strength S (length form), weighted oscillator strength gf (length form), transition rate A_{ki} (length form) in s^{-1}, δT accuracy indicator. CC + CV corresponds to calculations including core correlation (CC) and core-valence (CV) correlations. The importance of the CC + CV corrections are less important for higher Z so it have been neglected.

Upper State	λ (Å)	S	gf	A_{ki} (s^{-1})	δT
	Xe^{18+} ($Z = 54$)				
$4p^5 4d\ ^3P_1^o$	152.32	1.787×10^{-4}	3.564×10^{-4}	3.415×10^{7}	0.072
(CC + CV)	152.09	1.895×10^{-4}	3.785×10^{-4}	3.638×10^{7}	0.229
$4p^5 4d\ ^3D_1^o$	131.43	1.483×10^{-1}	3.427×10^{-1}	4.411×10^{10}	0.008
(CC + CV)	131.33	1.565×10^{-1}	3.620×10^{-1}	4.667×10^{10}	0.042
$4p^5 4d\ ^1P_1^o$	107.06	1.472	4.178	8.105×10^{11}	0.013
(CC + CV)	107.73	1.402	3.952	7.572×10^{11}	0.035
	Cs^{19+} ($Z = 55$)				
$4p^5 4d\ ^3P_1^o$	145.90	1.025×10^{-4}	2.133×10^{-4}	2.228×10^{7}	0.091
$4p^5 4d\ ^3D_1^o$	125.39	1.581×10^{-1}	3.829×10^{-1}	5.414×10^{10}	0.005
$4p^5 4d\ ^1P_1^o$	102.10	1.356	4.036	8.607×10^{11}	0.011
	Ba^{20+} ($Z = 56$)				
$4p^5 4d\ ^3P_1^o$	140.00	4.707×10^{-5}	1.021×10^{-4}	1.158×10^{7}	0.130
$4p^5 4d\ ^3D_1^o$	119.84	1.678×10^{-1}	4.253×10^{-1}	6.585×10^{10}	0.003
$4p^5 4d\ ^1P_1^o$	97.49	1.251	3.897	9.117×10^{11}	0.010
	Ce^{22+} ($Z = 58$)				
$4p^5 4d\ ^3P_1^o$	129.52	1.098×10^{-7}	2.576×10^{-7}	3.414×10^{4}	0.809
$4p^5 4d\ ^3D_1^o$	109.94	1.867×10^{-1}	5.158×10^{-1}	9.487×10^{10}	0.001
$4p^5 4d\ ^1P_1^o$	89.15	1.066	3.632	1.016×10^{12}	0.006
	Gd^{28+} ($Z = 64$)				
$4p^5 4d\ ^3P_1^o$	105.69	3.473×10^{-4}	9.980×10^{-4}	1.986×10^{8}	0.073
$4p^5 4d\ ^3D_1^o$	87.39	2.301×10^{-1}	7.996×10^{-1}	2.328×10^{11}	0.012
$4p^5 4d\ ^1P_1^o$	69.25	6.701×10^{-1}	2.939	1.363×10^{12}	0.003
	Hf^{36+} ($Z = 72$)				
$4p^5 4d\ ^3P_1^o$	84.65	1.640×10^{-3}	5.883×10^{-3}	1.826×10^{9}	0.063
$4p^5 4d\ ^3D_1^o$	67.45	2.431×10^{-1}	1.095	5.352×10^{11}	0.022
$4p^5 4d\ ^1P_1^o$	50.25	3.797×10^{-1}	2.295	2.021×10^{12}	0.011
	W^{38+} ($Z = 74$)				
$4p^5 4d\ ^3P_1^o$	80.68	2.036×10^{-3}	7.666×10^{-3}	2.619×10^{9}	0.055
$4p^5 4d\ ^3D_1^o$	63.64	2.397×10^{-1}	1.144	6.281×10^{11}	0.007
$4p^5 4d\ ^1P_1^o$	46.45	3.337×10^{-1}	2.182	2.248×10^{12}	0.0004
	Au^{43+} ($Z = 79$)				
$4p^5 4d\ ^3P_1^o$	71.88	3.041×10^{-3}	1.285×10^{-2}	5.530×10^{9}	0.069
$4p^5 4d\ ^3D_1^o$	55.24	2.252×10^{-1}	1.238	9.023×10^{11}	0.029
$4p^5 4d\ ^1P_1^o$	38.08	2.477×10^{-1}	1.975	3.028×10^{12}	0.014

III. LIFETIME TRENDS, $Z = 54$–79

Mathematically, the variable Z appearing in the Hamiltonian may be considered a real (rather than integer) variable. Then eigenstates for a specific (πJ) will be specified by their order and will vary smoothly with Z [22]. Thus the quantum numbers for smooth trends are π, J, and an index for the position (POS) of the state in spectrum of the Hamiltonian.

Figure 1 shows the composition of the wave function for two $J = 2$ states of odd parity, namely those in the first position (solid symbols) and fourth position (empty symbols) as a function of $1/(Z - 35)$. For this (πJ) there is a strong interaction between $^3P_2^o$ and $^3D_2^o$ CSFs for $4s^2 4p^5 4d$ and a weaker one with $^1D_2^o$ and $^3F_2^o$. There is a change in the largest component of the composition of the $J = 2$ (POS 4, empty symbols) ASF at a higher Z than the change in the lowest (POS 1, solid symbols). Notice that along each of the four lines, the composition varies smoothly in spite of a change of the largest component, from which it follows that atomic properties will also be continuous with respect to Z. For the $J = 1$ excited levels, in the present $Z = 54$–79 range, there is a change in the largest component for POS = 2 from $^3D_1^o$ to $^1P_1^o$ at higher Z than W^{38+} ($Z = 74$) or at Re($Z = 75$). Table III shows that the $^3D_1^o$ component of POS = 3 is increasing relative to $^1P_1^o$ and will become dominant at higher Z.

Though many atomic properties are continuous, the lifetime needs special consideration. When $E2$ and $M1$ transitions are omitted, the lifetimes τ of the $4p^5 4d\ (J = 1)$ levels are, by definition, $\tau = 1/A$. By Eq. (4), the formula for A is proportional to the transition energy (ΔE) and the square of the transition matrix element (ME). Thus, if the ME changes

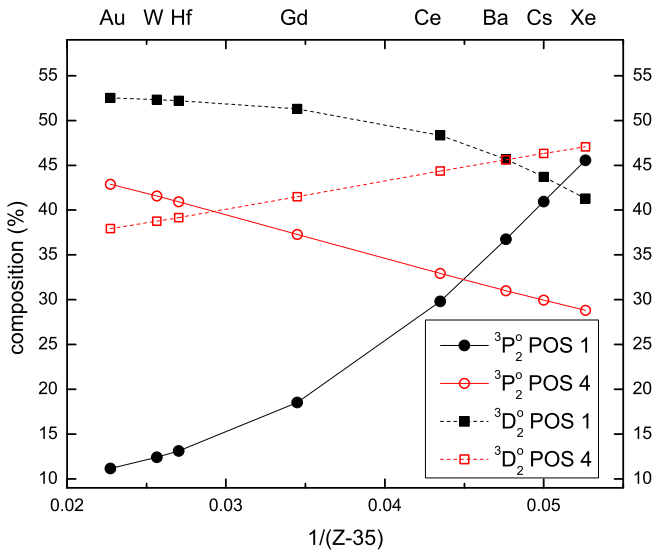

FIG. 1. (Color online) Contributions from the $^3P_2^o$ (circles) and $^3D_2^o$ (squares) CSFs to the $J = 2$ ASFs for position 1 (solid symbols, black online) and position 4 (empty symbols, red online).

sign, the lifetime ($\tau = 1/A$) as a function of Z may have a singularity, although in practice other transitions that are usually negligible in comparison to the $E1$ transition keep the lifetime from being infinite.

In the Table V, ME's in the length form are shown for the three $E1$ transitions. In LSJ coupling, contributions to the ME from the $^1S_0$ ground state come only from the $^1P_1^o$ component in the upper state. Table III shows that the composition of the $^3P_1^o$ state (POS = 1) includes less than 0.5% of $^1P_1^o$ composition, a negligible contribution not included in the table. Thus, from an LSJ perspective, a small line strength would be expected. For the $^3D_1^o$ (POS = 2) state the $^1P_1^o$ component is larger and increases with Z, whereas the $^1P_1^o$ (POS = 3) state has a large but decreasing $^1P_1^o$ component. However in jj coupling the three $4p^5 4d$ basis states are significant components in each state. Thus the small line strength [smaller by 4–2 orders of magnitude (Table IV)] for POS = 1 is achieved through numerical cancellation, which makes the results more sensitive to small changes [23]. Furthermore, Table V also shows that the matrix element changes sign and, for some Z (near $Z = 58$) the matrix element is zero and hence A also is zero. Near a zero, the otherwise negligible contributions to the lifetime

TABLE V. Matrix elements in the length form for $E1$ transitions between $4p^6\ ^1S_0$ and $4p^5 4d$ $J = 1$.

Z	POS 1	POS 2	POS 3
54	4.1268×10^{-4}	-1.3777×10^{-2}	-5.3296×10^{-2}
55	3.2623×10^{-4}	-1.4908×10^{-2}	-5.3638×10^{-2}
56	2.3043×10^{-4}	-1.6073×10^{-2}	-5.3942×10^{-2}
58	1.2032×10^{-5}	-1.8479×10^{-2}	-5.4456×10^{-2}
64	-8.2905×10^{-4}	-2.5807×10^{-2}	-5.5581×10^{-2}
72	-2.2493×10^{-3}	-3.4376×10^{-2}	-5.7660×10^{-2}
74	-2.6299×10^{-3}	-3.6174×10^{-2}	-5.8474×10^{-2}
79	-3.6074×10^{-3}	-4.0396×10^{-2}	-6.1447×10^{-2}

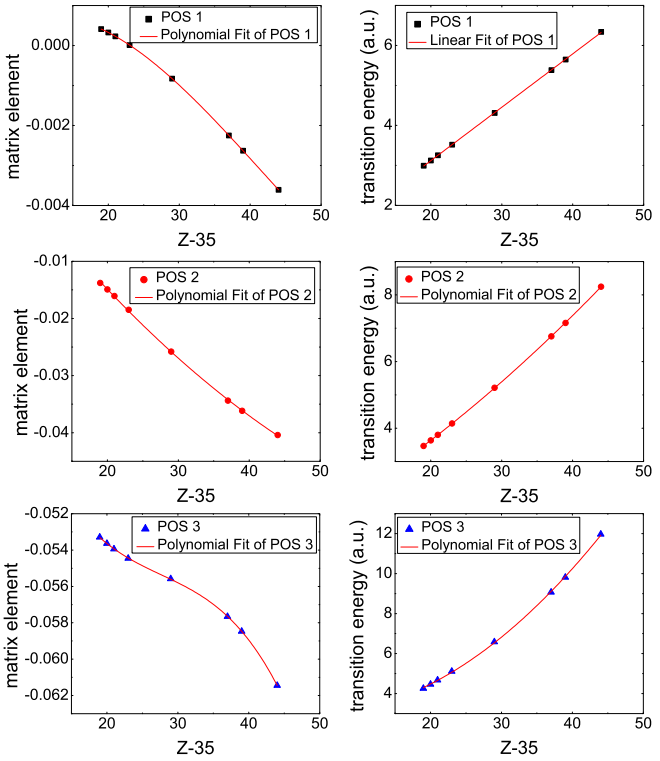

FIG. 2. (Color online) Matrix elements and transition energies for the $4p^6\ ^1S_0$- $4p^5 4d$ $J = 1$ transitions.

from $E2$ and $M1$ transitions become significant and define the lifetime.

The transition energies and matrix elements are shown in Fig. 2 as polynomials obtained from a least-squares fit of the numerical data, namely:

$$\begin{aligned}
1)\ \mathrm{ME} &= -3.433 \times 10^{-4} + 1.875 \times 10^{-4}(Z-35) - 9.159 \\
&\quad \times 10^{-6}(Z-35)^2 + 7.302 \times 10^{-8}(Z-35)^3, \\
\Delta E &= 0.4489 + 0.1336(Z-35), \\
2)\ \mathrm{ME} &= 0.01521 - 0.0017(Z-35) + 9.924 \\
&\quad \times 10^{-6}(Z-35)^2, \\
\Delta E &= 0.8140 + 0.1180(Z-35) + 0.00115(Z-35)^2, \\
3)\ \mathrm{ME} &= -0.03522 - 0.00182(Z-35) + 5.9087 \\
&\quad \times 10^{-5}(Z-35)^2 - 7.117 \times 10^{-7}(Z-35)^3, \\
\Delta E &= 2.9997 - 0.003382(Z-35) \\
&\quad + 0.00538(Z-35)^2.
\end{aligned}$$

The accuracy of the fit is determined by the parameter R^2. A value of R^2 close to 1 indicates that the fit is a good one.

Adjusted R^2 for each fit:

POS1: ME 1; ΔE 0.99995;
POS2: ME 0.99973; ΔE 0.99998;
POS3: ME 0.99995; ΔE 0.99973.

Finally, Fig. 3 shows the lifetime trends for the three $J = 1$ levels of $4p^5 4d$ as a function $1/(Z-35)$ and the computed values. The lines are derived from the polynomial fits to the data for the transition energies and the transition matrix elements, whereas the symbols represent the lifetimes reported in Table III from our computed results. Clearly evident is the long lifetime in the vicinity of Ce^{22+}.

IV. COMPARISON WITH EXPERIMENT

Table VI compares theoretical results computed for the purpose of line classification, the measured values, and present wavelengths from calculations assuming the inactive $3d^{10}$ core. For all $M1$ transitions between levels of $4p^5 4d$ our computed wavelengths are of similar or better accuracy than previously published theoretical values, except for the $4p^5 4d\,^3F_4^o - 4p^5 4d\,^3F_3^o$ transition in W^{38+} where our wavelength differs from observation by 2.5%. The reason for the discrepancy is not known. Of the $E1$ transitions, only two lines have been observed for transitions to the $^3P_1^o$ (POS = 1) levels,

TABLE VI. Comparison of computed wavelengths (λ in Å) from different theories with observed wavelengths. SE: semiempirical.

Lower	Upper	Th.	Exp.	This work
Xe^{18+} ($Z = 54$)				
$4p^5\,4d\,^3P_1^o$	$4p^5\,4d\,^3P_2^o$	4337[a]	4363(4)[a]	4333.78
$4p^6\,^1S_0$	$4p^5 4d\,^3D_1^o$		131.709[b]	131.43
			131.740[c]	
$4p^6\,^1S_0$	$4p^5 4d\,^1P_1^o$	104.91[d]	106.37[d]	107.06
		101.05[e]	108.35[e]	
			108.39[b]	
			108.409[c]	
Cs^{19+} ($Z = 55$)				
$4p^6\,^1S_0$	$4p^5 4d\,^3D_1^o$		125.718[c]	125.39
$4p^6\,^1S_0$	$4p^5 4d\,^1P_1^o$		103.368[c]	102.10
Ba^{20+} ($Z = 56$)				
$4p^6\,^1S_0$	$4p^5 4d\,^3D_1^o$		120.183[SE][f]	119.84
$4p^6\,^1S_0$	$4p^5 4d\,^1P_1^o$		98.666[SE][f]	97.49
Ce^{22+} ($Z = 58$)				
$4p^6\,^1S_0$	$4p^5 4d\,^3D_1^o$		110.353[SE][c]	109.94
$4p^6\,^1S_0$	$4p^5 4d\,^1P_1^o$		90.146[SE][c]	89.15
Hf^{36+} ($Z = 72$)				
$4p^6\,^1S_0$	$4p^5 4d\,^3D_1^o$	67.3306[g]	67.79(3)[g]	67.45
W^{38+} ($Z = 74$)				
$4p^5 4d\,^3P_1^o$	$4p^5 4d\,^3D_2^o$	2758.80[h]		2907.15
$4p^5 4d\,^3F_3^o$	$4p^5 4d\,^3F_4^o$	798.08[h]	799.23[h]	779.46
$4p^5 4d\,^3P_1^o$	$4p^5 4d\,^1D_2^o$	585.99[h]		591.72
$4p^5 4d\,^3D_2^o$	$4p^5 4d\,^3D_3^o$	556.76[h]	559.04[h]	559.16
$4p^5 4d\,^3F_3^o$	$4p^5 4d\,^3D_3^o$	523.67[h]	532.87[h]	531.66
$4p^5 4d\,^3F_3^o$	$4p^5 4d\,^3F_2^o$	138.09[h]		138.68
		138.0184[i]		
$4p^5 4d\,^3F_4^o$	$4p^5 4d\,^1F_3^o$	128.05[h]		129.26
		127.9788[i]		
$4p^6\,^1S_0$	$4p^5 4d\,^3P_1^o$	80.8856[i]	80.6420(226)[j]	80.68
		80.897[h]		
$4p^6\,^1S_0$	$4p^5 4d\,^3D_1^o$	63.3262[i]	63.8834(41)[j]	63.64
		63.249[h]	63.98[h]	
$4p^6\,^1S_0$	$4p^5 4d\,^1P_1^o$	46.1417[i]	46.6703(12)[j]	46.45
		46.064[h]	46.40[h]	
Au^{43+} ($Z = 79$)				
$4p^6\,^1S_0$	$4p^5 4d\,^3P_1^o$	71.815[g]	71.93(2)[g]	71.88
$4p^6\,^1S_0$	$4p^5 4d\,^3D_1^o$	55.183[g]	55.51(2)[g]	55.24
		55.01[k]	55.46[k]	
$4p^6\,^1S_0$	$4p^5 4d\,^1P_1^o$	37.89[k]	38.27[k]	38.08

[a] Crespo *et al.* [7].
[b] Kato *et al.* [6].
[c] Sugar *et al.* [8].
[d] Breton *et al.* [4].
[e] Biedermann *et al.* [5].
[f] Sansonetti *et al.* [24].
[g] Draganić *et al.* [9].
[h] Radtke *et al.* [3].
[i] Fournier [25].
[j] Utter *et al.* [1].
[k] Träbert *et al.* [10].

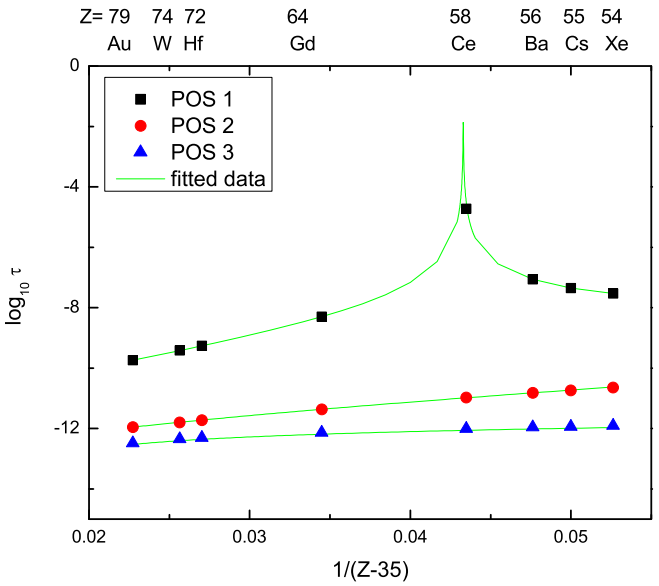

FIG. 3. (Color online) Lifetime trends of the three $J = 1$ levels of $4p^5 4d$ as a function $1/(Z - 35)$.

namely W^{38+} and Au^{43+}. For both these transitions, present results are in better agreement (0.07%) with observation than previous theory. For transitions to POS = 3, Biedermann *et al.* [5] claimed that the line ($\lambda = 106.37$ Å) for Xe^{18+} was not identified correctly by Breton *et al.* [4]. Omitting this value, and comparing only transitions to $^3D_1^o$ and $^1P_1^o$, present wavelengths agree with observed to within 0.5% except for transitions to $^1P_1^o$ at the lower end of our range where the discrepancy may be as large as 1.2%. For Xe^{18+}, Table IV showed that the CC + CV calculation reduced the discrepancy to 0.6%. The importance of the CC + CV corrections decreases with the degree of ionization: wavelengths without this correction agree with observed to within 0.5% at $Z = 79$. At the same time, the present theoretical wavelengths are always shorter than the experimental ones or, equivalently, the computed transition energies are too large.

V. CONCLUSIONS

Results from SRSD-MCDHF calculations have been reported for some Kr-like ions in the range $Z = 54$–79 assuming an inactive Ni-like core. Although there is excellent convergence in wavelengths and length or velocity values of the transition rate, computed wavelengths for transitions from the ground state to $4p^5 4d$ excited states are systematically shorter than observed values. A test for Xe^{18+} showed that including CC + CV effects from $3d^{10}$ improved agreement for the $^1P_1^o$ level but had little effect on the lower two $J = 1$ levels. It is customary to think of the $3d^{10}$ subshell as being farther from nucleus than the $3s^2 3p^6$ subshells. In fact, the mean radii for $\{3s, 3p_-, 3p, 3d_-, 3d\}$ are $\{0.301, 0.293, 0.304, 0.275, 0.278\}$ respectively for $Z = 74$. Thus the $3d$ subshell is the closest to the nucleus. CC + CV effects from $3s^2 3p^6$ need to be investigated in order to better understand the source of the discrepancy with observation.

The LS coupling scheme has an advantage for transition rates in that transitions can be readily classified as LS allowed or LS forbidden where, in relativistic calculations, the latter are accompanied by extensive cancellation. However, LS labels are not appropriate for the study of isoelectronic sequences for complex, heavy ions. We have shown that, by defining sequences for a given number electrons and the quantum numbers of π, J, and sequential level index POS, the composition of wave functions varies smoothly and energy levels and matrix elements can be approximated accurately by analytic functions of nuclear charge Z. A lifetime may become exceedingly large when a transition matrix element is in the vicinity of a zero.

[1] S. B. Utter, P. Beiersdorfer, and E. Träbert, Can. J. Phys. **80**, 1503 (2002).

[2] Yu. Ralchenko, J. Reader, J. M. Pomeroy, J. N. Tan, and J. D. Gillaspy, J. Phys. B **40**, 3861 (2007).

[3] R. Radtke, C. Biedermann, G. Fussmann, J. L. Schwob, P. Mandelbaum, and R. Doron, Atomic and Plasma Material Interaction Data for Fusion **13**, 45 (2007).

[4] C. Breton, C. DeMichelis, W. Hecq, M. Mattioli, J. Ramette, and B. Saoutic, Phys. Scr. **37**, 33 (1988).

[5] C. Biedermann, R. Radtke, G. Fussmann, J. L. Schwob, and P. Mandelbaum, Nucl. Instrum. Methods Phys. Res., Sect. B **235**, 126 (2005).

[6] T. Kato, H. Funaba, K. Sato, D. Kato, M.-Y. Song, N. Yamamoto, H. Tanuma, H. Ohashi, A. Sasaki, F. Koike, K. Nishihara, K. Fahy, and G. O'Sullivan, J. Phys. B **41**, 035703 (2008).

[7] J. R. Crespo López–Urrutia, P. Beiersdorfer, K. Widmann, and V. Decaux, Can. J. Phys. **80**, 1687 (2002).

[8] J. Sugar, V. Kaufman, and W. L. Rowan, J. Opt. Soc. Am. B **8**, 2026 (1991).

[9] I. N. Draganić, Y. Ralchenko, J. Reader, J. D. Gillaspy, J. N. Tan, J. M. Pomeroy, S. M. Brewer, and D. Osin, J. Phys. B **44**, 025001 (2011).

[10] E. Träbert, P. Beiersdorfer, K. B. Fournier, S. B. Utter, and K. L. Wong, Can. J. Phys. **79**, 153 (2001).

[11] See Supplemental Material at http://link.aps.org/supplemental/10.1103/PhysRevA.91.022509 for $E2$ and $M1$ data.

[12] P. Jönsson, G. Gaigalas, J. Bieroń, C. Froese Fischer, and I. P. Grant, Comput. Phys. Commun. **184**, 2197 (2013).

[13] Z. Rudzikas, *Theoretical Atomic Spectroscopy*, 2nd ed. 2007 (Cambridge University Press, Cambridge, 1997).

[14] I. P. Grant, *Relativistic Quantum Theory of Atoms and Molecules* (Springer, Berlin, 2007).

[15] F. A. Parpia, C. Froese Fischer, and I. P. Grant, Comput. Phys. Commun. **94**, 249 (1996).

[16] I. P. Grant, B. J. McKenzie, P. R. Norrington, D. F. Mayers, and N. C. Pyper, Comput. Phys. Commun. **21**, 207 (1980).

[17] I. P. Grant, J. Phys. B **7**, 1458 (1974).

[18] C. Froese Fischer, Phys. Scr., T **134**, 014019 (2009).

[19] C. Froese Fischer, J. Phys. B **43**, 074020 (2010).

[20] J. Ekman, M. R. Godefroid, and H. Hartman, Atoms **2**, 215 (2014).
[21] C. Froese Fischer and G. Tachiev, Atomic Data and Nucl. Data Tables **87**, 1 (2004).
[22] C. Froese Fischer, Phys. Rev. A **22**, 551 (1980).
[23] A. Ynnerman and C. F. Fischer, Phys. Rev. A **51**, 2020 (1995).
[24] J. E. Sansonetti and J. J. Curry, J. Phys. Chem. Ref. Data **39**, 043103 (2010).
[25] K. B. Fournier, At. Data Nucl. Data Tables **68**, 1 (1998).